Process Safety and Environmental Protection 170 (2023) 728–737

Contents lists available at ScienceDirect

Process Safety and Environmental Protection

journal homepage: www.journals.elsevier.com/process-safety-and-environmental-protection

Experimental study on the effects of salt solution pH on the performance of reverse electrodialysis stack

Lu Wang, Yanan Zhao, Xi Chen, Rui long *, Zhichun Liu, Wei Liu

School of Energy and Power Engineering, Huazhong University of Science and Technology, Wuhan 430074, China

ARTICLE INFO

Keywords:
Reverse electrodialysis
Salinity gradient energy
Solution pH
Energy conversion

ABSTRACT

Reverse electrodialysis (RED) is a promising way of harvesting salinity gradient energy (SGE). The seawater or industrial wastewater may have various pHs. Here the RED performance involving sodium salt solutions with different ion valence ratios including anions of Cl^-, SO_4^{2-}, and PO_4^{3-} is experimentally investigated in symmetric and asymmetric pH configurations. In the symmetrical pH configuration, increasing the solution pH significantly weakens the energy conversion performance for the 1:1 and 1:3 salts; for the 1:2 salt, the power density and energy conversion efficiency increase and then decrease with increasing pH due to the coupling effects of OH^- on the ion transportation through AEMs and CEMs. In the asymmetric pH configuration, increasing the pH of the low concentration solution decreases the power density and energy conversion efficiency. As the pH of the high concentration solution increases, the output power and energy conversion efficiency decrease and then increase for the 1:1 salt due to the coupling effects of the ion transmembrane concentration difference and OH^- on the ion migration of IEMs; for the 1:2 salt, the output power and energy conversion efficiency increase and then decrease; for the 1:3 salt, OH^- inhibits the hydrolysis of Na_3PO_4 and anion migration, leading to the lowered output power density and energy efficiency.

1. Introduction

Huge energy consumption intensifies the depletion of traditional fossil energy sources. It's imperative to promote sustainable energy utilization, thus relieving energy-related social and environmental issues. The salinity gradient energy (SGE) is a kind of potential future energy generated from the electrochemical potential difference between electrolyte solutions with different concentrations (Logan and Elimelech, 2012; Lacey, 1980). It is a completely clean and renewable energy resource (Li et al., 2022), with high safety and no harmful substances generated during the utilization processes which include desalination and wastewater treatment (Panagopoulos, 2021; Soliman et al., 2021; Guo et al., 2022; Mukherjee et al., 2022). Natural SGE derived from the salinity difference between fresh water and seawater widely exists, meanwhile, artificial SGE sourced from industrial or domestic wastewater with high salinity also presents great potential (Tufa et al., 2018; Daniilidis et al., 2014). The energy theoretically available from the global salinity gradient is about 1.4–2.6 TW based on the discharges of rivers into oceans (Veerman et al., 2010a). The most mature technologies for harvesting SGE are pressure retarded osmosis (PRO) and reverse electrodialysis (RED) (Hong et al., 2015; Yip et al., 2016; Venzke et al., 2018), both have developed laboratory demonstration and pilot systems (Tedesco et al., 2017). There have been some pilot RED plants, such as a pilot plant built in the Netherlands in 2014 with a target generation power of 50 kW (Cipollina et al., 2016), and a factory built in Italy under the European project REAPower, which is capable of generating 1 kW of gross power by using brines, brackish water and municipal treated wastewater (Tedesco et al., 2016).

The principle of RED was first introduced by Pattle in 1954 (Pattle, 1954). The RED system consists of a membrane stack and two electrodes, where the membrane stack includes alternately piled cation exchange membranes (CEMs) and anion exchange membranes (AEMs), with woven spacers between them to form high and low concentration solution compartments (Jang et al., 2020). The charged groups inside these membranes make CEMs selective for cations, while AEMs allow only anion migration. Driven by the transmembrane concentration gradient, cations and anions in the concentrated solution permeate into the dilute solution through CEMs and AEMs respectively, and then an

* Corresponding author.
E-mail addresses: l_wang@hust.edu.cn (L. Wang), yn_zhao@hust.edu.cn (Y. Zhao), cx413@hust.edu.cn (X. Chen), r_long@hust.edu.cn (R. long), zcliu@hust.edu.cn (Z. Liu), w_liu@hust.edu.cn (W. Liu).

https://doi.org/10.1016/j.psep.2022.12.034
Received 23 September 2022; Received in revised form 2 December 2022; Accepted 9 December 2022
Available online 15 December 2022

ionic current is generated (Veerman et al., 2010b). Subsequently, a redox reaction occurs at the cathode and anode. An electric current can be collected when the RED stack is connected to an external circuit.

Most research on RED systems involving macro and micro aspects has been mainly focused on stack configurations (Long et al., 2018a, 2021; Kuang et al., 2019), operating conditions (Ortiz-Imedio et al., 2019; Zhu et al., 2015; Long et al., 2018a), and membrane properties (Hong et al., 2019; Długołęcki et al., 2010; Pawlowski et al., 2017). There were also a few studies aimed to optimize energy conversion performance by investigating heat transfer and thermal diffusion phenomena in the SGE harvest process (Long et al., 2020, 2019). In addition, solution properties can also significantly impact energy conversion performance. Such as multivalent ions and natural organic matter in feed solutions can weaken the membrane permselectivity and RED performance (Avci et al., 2016; Kingsbury et al., 2017), positive and negative temperature gradients between inlet solutions show different effects on power efficiency (Long et al., 2018b; Cui et al., 2022), and rising solutions' temperature would enhance the power density of the RED stack (Benneker et al., 2018; Guo et al., 2018).

Among diverse influencing factors, figuring out the effects of solution pH is also demanding. Chen et al (Chen et al., 2022). studied the performance of nanopore channels on SGE extraction by changing the pH of inlet and outlet solutions, and showed that the pH on the low concentration side had a significant effect on energy conversion. Hsu et al (Hsu et al., 2017). investigated a pH-regulated conical nanopore and found that the farther the pH deviated from neutral resulted in an increase in the surface charge density, which contributed to the ion selectivity of the nanopore and the output power. Subsequently, they focused on the effect of the non-uniform distribution of H^+ to gather information desirable and necessary for designing RED devices (Hsu et al., 2019). Mai et al (Mai and Yang, 2020). found that the output power increased when the pH of the nanopore increased from 5 to 10, while the polarization of the ion concentration significantly led to a decrease in power generation after pH reached 11. Culcasi et al (Culcasi et al., 2021). developed a multi-scale model to predict the performance of the sustainable recovery of energy from pH gradients of industrial wastewater and got promising net power densities.

However, most of the previous studies on the effect of pH on SGE conversion performance have only focused on the microscopic level such as analyzing the power generation performance of individual nanochannels or numerical studies, while few papers had experimentally studied the effect of pH on the performance of macroscopic RED stacks. Kingsbury et al (Kingsbury et al., 2017). compared the RED performance of five real water pairs to that of synthetic controls and found that the pickling brine/stormwater pair showed better performance than controls, and they attributed this unique behavior to coupling effects of the pH gradient and organic matter. The solution pH may have specific impacts on the RED process, and it is meaningful to systematically investigate those effects on the energy conversion performance of macroscopic RED stacks.

In this paper, a RED stack consisting of five-cell pairs was constructed. Three common sodium salts with different ion valence ratios (NaCl, Na_2SO_4, and Na_3PO_4) which hardly react with acid and alkali solutions, were adopted to figure out the effects of pH on diverse salt solution pairs. Adjusting the pH of high and low concentration solutions simultaneously or independently induces the RED stack to work in different operating configurations: symmetric pH configuration (same pH of high and low concentration solutions) and asymmetric pH configuration (different pH of high and low concentration solutions), and the effects of pH on the open-circuit voltage, total resistance, output power density and energy conversion efficiency of the RED stack were systematically analyzed and discussed. This study may provide new sights into the efficient extraction process of SGE at adjustable pHs or different pH gradients.

2. Materials and methods

2.1. RED stack

Here, a RED stack with five pairs of ion exchange membranes (IEMs) was set up. Each cell pair contained one CEM (HoCM Grion-0014) and one AEM (HoAM Grion-1204). Alternative arrangements of AEMs and CEMs were separated by polyvinyl chloride woven spacers (with a thickness of 0.23 mm) and silicone gaskets (with a thickness of 0.8 mm) combination. All of the membranes and the spacers were provided by Hangzhou Lvhe Environmental Protection Technology Co., Ltd. The relevant properties of IEMs are listed in Table 1, and the main specifications of the spacer are listed in Table 2.

An additional CEM was arranged as a shielding membrane between the cell pair units and the electrodes, which could avoid contamination of AEMs by anions in the electrode rinse solution (ERS) and interference with ion migration. Two titanium alloy plates covered with acid- and alkali-resistant coatings were used as anode and cathode, respectively. The PVC polar water plates where the electrode plates were installed acted as polar water chambers to provide the current path for the stack. Bolts and two steel plates covered with corrosion-resistant coating were used to assemble the whole stack. The external dimension of the stack was 297 cm^2 (11 cm × 27 cm), while the effective internal size for ion migration was 112 cm^2. Fig. 1 shows the schematic of the experimental system.

2.2. Salt solutions

Three sodium salts with anions at different valences (NaCl, Na_2SO_4 and Na_3PO_4) were dissolved in deionized water respectively to prepare high and low concentration solutions for the RED stack. The concentrations of the high and low concentration solutions are set to 0.5 M and 0.017 M, respectively. The electrode rinse solution (ERS) consisted of 0.05 M $K_3Fe(CN)_6$, 0.05 M $K_4Fe(CN)_6$ and 0.25 M NaCl. Where adding NaCl can limit the transfer of water to ERS (Hulme et al., 2021) and enhance the conductivity of the solution (Zhang et al., 2021). Considering the less variation of the concentration of OH^- within adjacent pH values and in order to present obvious trends in results, a larger pH variation step of $\Delta pH = 2$ is designed and employed. NaOH (purity: ≥96%) and HCl (purity: 36.0–38.0%) were prepared into extremely dilute solutions, 0.01 M solutions, and 1 M solutions or dissolved in salt solutions directly to tune the feed solutions' pH to 7, 9, 11, and 13 with little change in the original volume. All electrolytes mentioned above were offered by Sinopharm Chemical Reagent Co., Ltd.(SCR), with the purity level of analytical reagent (AR).

2.3. Experimental procedures

Two peristaltic pumps (BT100–2 J, LongerPump, China) were used to pump the high and low concentration solutions through the RED stack with a flow rate of 100 $mL \cdot min^{-1}$. Another peristaltic pump was used to circulate ERS along the electrodes with a flow rate of 200 $mL \cdot min^{-1}$. The high and low concentration salt solutions and effluent streams were held in transparent beakers, respectively, while ERS was stored in a brown glass bottle to avoid the decomposition of hexacyanoferrate by light. A pH meter (FE28-Meter, Mettler Toledo, China) was used to measure and control the pH values of the prepared solutions with an adjustment accuracy of ± 0.1. The performance of the stack was evaluated by an electrochemical workstation (PGSTAT204, Metrohm Autolab, China), where the reference electrode (RE) and the counter electrode (CE) were connected to the stack cathode, and the sense (S) and the working electrode (WE) were connected to the anode, thus to form a measurement loop. The experiments were performed at room temperature(297 ± 1 K). The experimental system is shown in Fig. 2.

Experimental testing instruments, corresponding modes, tested parameters, accuracy, and uncertainty are listed in Table 3. The main

Table 1
Relevant properties of ion exchange membranes.

Membrane	Type	Thickness (mm)	Exchange capacity (mEq·g^{-1} (dry))	Area resistance (Ω·cm^2)	Permselectivity (%)	Moisture content (%)
HoCM G-0014	CEM	0.16	1.8–2.2	1.5–2.5	95–99	33–40
HoAM G-1204	AEM	0.16	1.8–2.0	3	90–95	24–28

Table 2
Main specifications of the spacer.

Spacer material	Thickness (mm)	Porosity (%)	Shadow fraction (%)
PVC	0.23	54	46

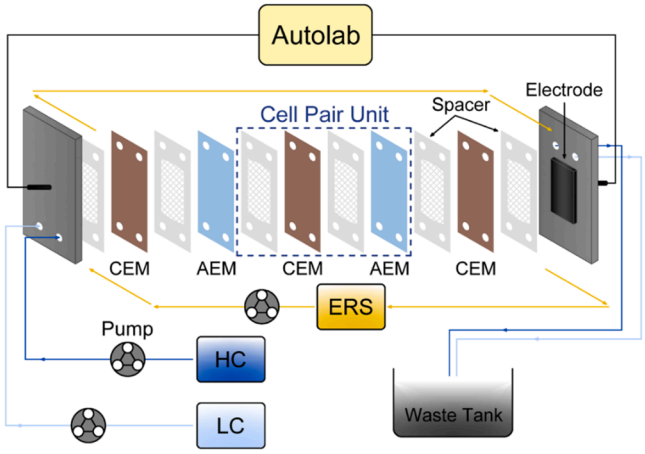

Fig. 1. Schematic of the experimental system.

sources of experiment errors are pH measurement errors, electrochemical workstation input current errors, electrochemical workstation potential measurement errors, and balance weighing errors.

Before the formal measurement, the high and low concentration salt solutions and the ERS were pumped into the RED stack with the set flow rates to flush the flow channels, respectively. Connect the measurement circuit until all flow chambers are filled with solutions and the ion transmembrane process tends to be stable, usually within 3 min. The OCV module was selected first to get the open-circuit voltage value of the RED stack, where the sampling interval was set to 0.1 s and the voltage gradient was limited to 1E-06 until reaching a stable result, typically within 5 min. Then the output voltage, total resistance and output power of the RED stack at different currents were determined by using chronopotentiometry, where the current range was chosen from 0 to − 0.14 A in steps of − 0.02 A. And each current was maintained for 30 s with a sampling interval of 0.3 s Fig. 3 shows the time-depended potential and current obtained by chronopotentiometry.

The theoretical open-circuit voltage (OCV) can be calculated according to the Nernst equation (Tedesco et al., 2015)

$$OCV = \frac{NRT}{F}\left(\frac{\alpha_{CEM}}{z_{pi}}\ln\frac{\gamma_{H,pi}C_H}{\gamma_{L,pi}C_L}+\frac{\alpha_{AEM}}{z_{ni}}\ln\frac{\gamma_{H,ni}C_H}{\gamma_{L,ni}C_L}\right) \quad (1)$$

where N is the number of cell pairs; R is the universal gas constant, 8.314 J·mol^{-1}·K^{-1}; T is the temperature(K); F is the Faraday constant, 96485 C·mol^{-1}; α_{CEM} and α_{AEM} are the permselectivity of cation and anion exchange membranes, respectively; z is the charge valence of ion, where the subscript '*pi*' represents positive ion and the subscript '*ni*' represents negative ion; C is the concentration(mol·L^{-1}), where the subscript '*H*' represents high concentration and the subscript '*L*' represents low concentration; γ is the activity coefficient, which can be determined by the Debye Hückel equation (Pitzer and Mayorga, 1993).

The output voltage of the RED stack is

$$E = OCV - IR_{total} \quad (2)$$

where I is the discharge current of the stack (A); R_{total} is the measured resistance (Ω).

The gross power is calculated as the product of the output voltage and the current, and the RED stack has the maximum output power when the external resistance is equal to the internal resistance of the stack

$$P_{\max} = \max(EI) = \frac{OCV^2}{4R_{total}} \quad (3)$$

The theoretical power available is the variation of Gibbs free energy

Table 3
Instrument parameter and uncertainty.

Instrument	Mode	Tested parameter	Accuracy	Uncertainty
Electrochemical workstation	PGSTAT204	Current	±0.2%	0.2% of the chosen range
		Potential	±0.2%	2 mV
pH meter	FE28-Meter	pH value	±0.01 pH	0.0152 pH
Balance	ME204	mass	0.1 mg	0.2 mg

Fig. 2. Experimental system of the RED stacks.

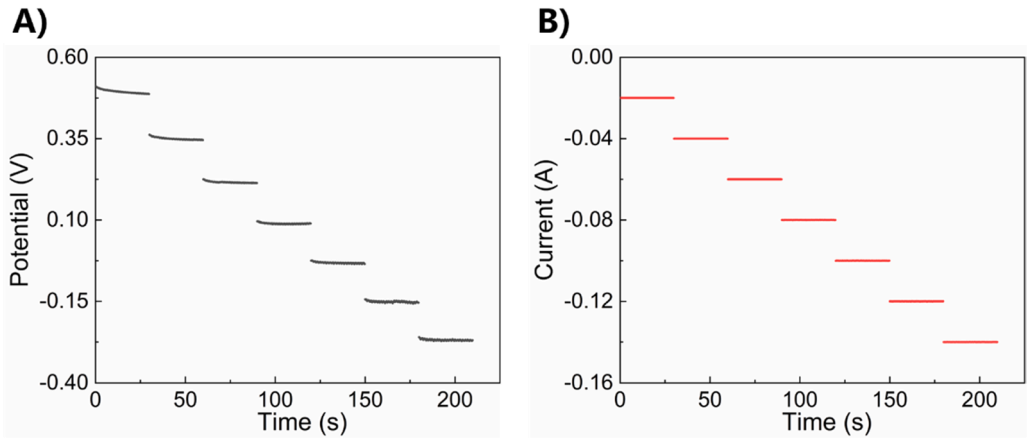

Fig. 3. Results of the chronopotentiometry.

of the mixing process (Choi et al., 2021), which can be calculated as

$$P_{\triangle G} = nRT\left(Q_L C_L \ln \frac{\gamma_L C_L}{\gamma_M C_M} + Q_H C_H \ln \frac{\gamma_H C_H}{\gamma_M C_M}\right) \tag{4}$$

$$c_M = \frac{Q_L C_L + Q_H C_H}{Q_L + Q_H} \tag{5}$$

where n is the number of ions obtained by the complete dissociation of one electrolyte molecule; Q is the volumetric flow rate of each feed solution ($L{\cdot}s^{-1}$); the subscript 'M' indicates the solution after total mixing.

The net energy efficiency is the ratio of the net power generated by the RED stack relative to the theoretical power (Kim et al., 2021), which can be calculated as

$$\eta_{\text{net}} = \frac{P - P_{pump}}{P_{\triangle G}} \times 100\% \tag{6}$$

$$P_{\text{pump}} = \Delta p_H Q_H + \Delta p_L Q_L \tag{7}$$

where P_{pump} is the power loss (W); Δp is the pressure drop of the salt solution (Pa).

3. Results and discussion

3.1. Performance in the symmetric pH configuration

In the symmetric pH configuration, the pHs of high and low concentration solutions are kept the same, which are adjusted from 7 to 13.

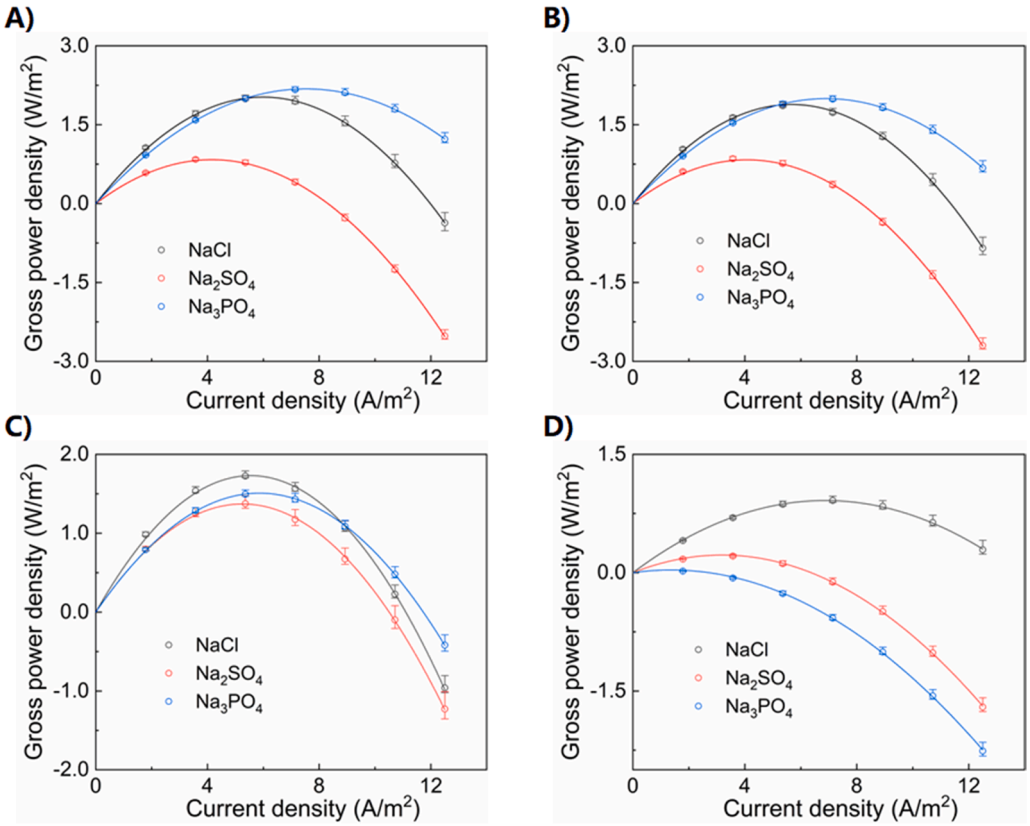

Fig. 4. Gross power density with the current density. A) pH = 7, B) pH = 9, C) pH = 11, and D) pH = 13.

Fig. 4 shows the variations of the RED stack's output power density with current density in different symmetric pH configurations. The errors of relevant parameters are indicated by the error bars. The output power density increases with increasing current density first, reaches its maximum and then decreases. When the current density exceeds a certain value, the power density changes its sign, as the discharge current set in chronopotentiometry is too large, converting the RED stack from the discharge state to the charge state. At a low salt solution pH (pH<11), when the RED system works at a low current density, the power density of the stack with NaCl solution is greater than that with Na_3PO_4 solution, while the power density of the stack with Na_2SO_4 solution presents the lowest value. When the RED system works at a larger current density, the stack with Na_3PO_4 solution has the greatest output power, followed by the stack with NaCl solution and Na_2SO_4 solution. As shown in Fig. 4D, when the pH is high (pH=13), the gross power of the stack with NaCl solution is the largest at different current densities, while that with Na_3PO_4 solution is the lowest and with a short circuit current density of 2.715 $A{\cdot}m^{-2}$. It indicates that the effects of salt solutions on the performance of RED stacks depend on the applied current density ranges. It is important to consider the actual operating current of RED stacks when feeding with different work salt solutions.

Fig. 5A illustrates the variations of open-circuit voltage with pHs under different salt solutions. At a lower pH (pH<11), the open-circuit voltage corresponding to different salt solutions lies in the following order: NaCl>Na_3PO_4 >Na_2SO_4. At a higher pH (pH>11), the open-circuit voltage of the RED stack with Na_2SO_4 solution surpasses that with Na_3PO_4 solution. As the pH increases, the open-circuit voltage of the stack with NaCl or Na_3PO_4 solution decreases slowly first, and then drops dramatically, while that of the stack with Na_2SO_4 solution increases first, achieving a peak value of 0.535 V at pH= 11 and then decreases. For the NaCl solution, the addition of Na^+ when adjusting pH can significantly decrease the transmembrane ion concentration difference thus weakening the transport driving force of ions, and reducing the output voltage of the RED stack. This phenomenon is particularly pronounced at higher pH levels. While for the Na_2SO_4 and Na_3PO_4 solutions which have higher concentrations of Na^+, the impact of Na^+ added is less important. For the RED stack with Na_2SO_4 solution, the permselectivity of IEM has a dominant effect on the open-circuit voltage in the symmetric pH configuration, and average permselectivities were calculated to 0.749, 0.776, 0.929, and 0.325 at pH from 7 to 13 according to Eq. (1). The presence of OH^- facilitates the migration of ions through IEMs at lower pHs, thus improving the open-circuit voltage of the stack; at higher solution pH (pH=13), the excessive concentration of OH^- weakens the permselectivity, coupling with the decreased transmembrane concentration ration induced by extra cations added, which lead to a decrease in the open-circuit voltage. For the RED stack with Na_3PO_4 solution, the addition of OH^- also inhibits the hydrolysis of Na_3PO_4 and weakens the migration of PO_4^{3-} through AEMs, resulting in the lowered open-circuit voltage of the stack.

Fig. 5B shows the variations of resistance with pHs under different salt solutions. At lower solution pHs, the resistance of the RED stack corresponding to different salt solutions lies in the order: NaCl>Na_2SO_4 >Na_3PO_4. At a higher pH (pH=13), the resistance of the stack with Na_2SO_4 solution is the largest, followed by that with NaCl solution and Na_3PO_4 solution. The resistance of the RED stack with different salt solutions increases with increasing solution pH, reaches a maximum value, and then decreases. For the stack with NaCl solution and Na_3PO_4 solution, the maximum resistances occur at pH= 11, which are 5.93 Ω and 4.05 Ω respectively. For the stack with Na_2SO_4 solution, the peak value of total resistance (5.04 Ω) appears at pH= 9.

Fig. 5C and D illustrate the maximum power density and energy conversion efficiency of the RED stack with solution pHs under different salt solutions, respectively. The maximum output power depends on the open-circuit voltage and the total resistance of the RED stack. At low solution pHs (pH<11), the stack with Na_3PO_4 solution has the largest maximum power density, while that with Na_2SO_4 solution is the lowest.

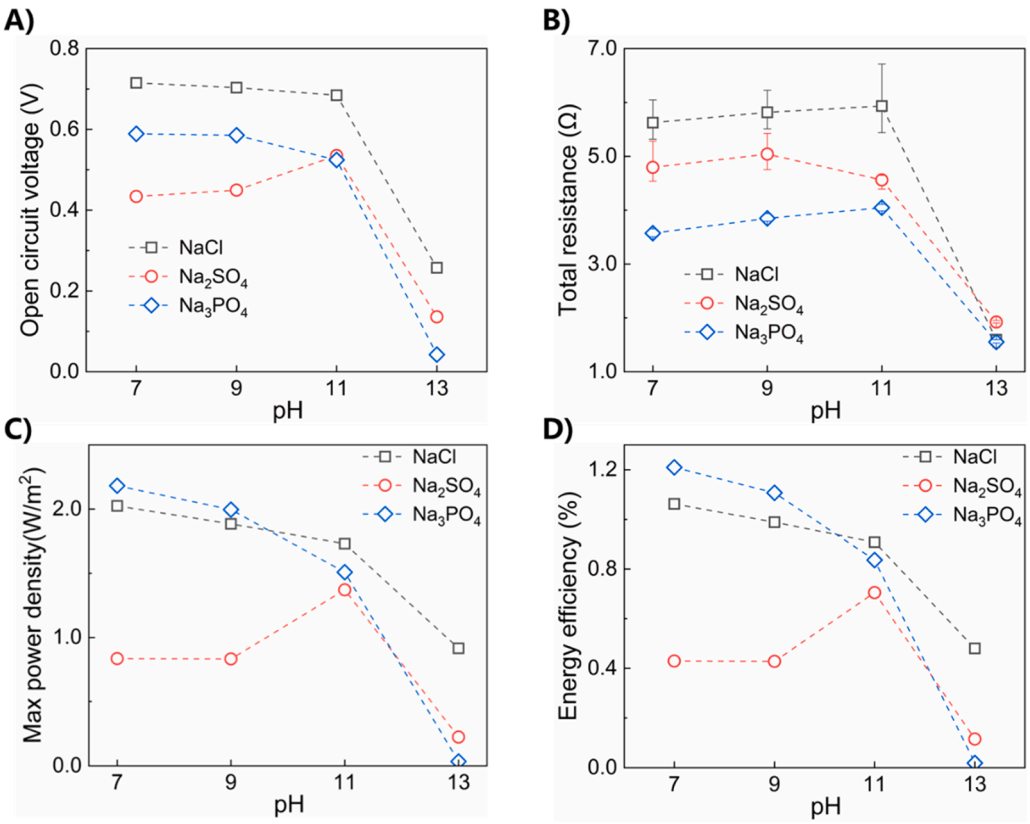

Fig. 5. Performance of the RED stack in symmetric pH configuration.

At larger solution pHs (pH≥11), the maximum output power of the stack with NaCl solution surpasses that with the other two salt solutions. The maximum power density of the stack with Na_3PO_4 solution presents the lowest at pH= 13. For the stack with Na_3PO_4 solution and NaCl solution, the maximum power densities are 2.18 $W{\cdot}m^{-2}$ and 2.02 $W{\cdot}m^{-2}$ at pH= 7, respectively, which gradually decreases as the solution pH increases. The maximum power density of the stack with Na_2SO_4 solutions increases first with increasing solution pH, achieves a peak value of 1.37 $W{\cdot}m^{-2}$ at pH= 11, and then decreases. In this experiment, the inlet flow rates and the concentrations of salt solutions are kept the same for different salt solutions. The input Gibbs free energy varies rather slightly, resulting in the energy conversion efficiency of the RED stack with different salt solutions presenting the same trend with the maximum power density. For the stack with Na_3PO_4 solution and NaCl solution, the energy conversion efficiencies are 1.21% and 1.06% at pH= 7, respectively, which gradually decreases as the solution pH increases. The energy conversion efficiency of the stack with Na_2SO_4 solution increases and then decreases with increasing pH, achieving a peak value of 0.71% at pH= 11. At lower pHs (pH<11), the stack with Na_3PO_4 has the largest energy conversion efficiency, while that with Na_2SO_4 solution is the worst. At higher pHs (pH≥11), the energy conversion efficiency of the stack with NaCl solution exceeds that with other two salt solutions. The energy efficiency of the stack with Na_3PO_4 solution presents the lowest value at pH= 13.

3.2. Performance in the asymmetric pH configuration

3.2.1. Effects of pH of the low concentration solution

Here the pH of the high concentration solution is kept at 7, and the pH of the low concentration solution is adjusted from 7 to 13. Fig. 6 shows the variations of the RED stack's output power density with current density under different pH values of the low concentration solution. When the pH of the low concentration solution is low(pH_L<11), under small current density conditions, the power density of the RED stack with NaCl solution is larger than that with Na_3PO_4 solution, and the power density of the stack with Na_2SO_4 solution is the smallest; when operating at larger current densities, the power density of the stack with Na_3PO_4 solution is the greatest, followed by the stack with NaCl solution and Na_2SO_4 solution. When the pH of the low concentration solution is large (pH≥11), the power density of the RED stack with Na_3PO_4 solution is the largest, and that with Na_2SO_4 solution presents the lowest value. In addition, when the pH of the low concentration solution increases to 13, the RED stack with NaCl or Na_2SO_4 solutions exhibits an extremely small output power density, and can only carry a low discharge current. The Na_3PO_4 solution is more adaptive to the harsh environment where the low concentration solution is strongly alkaline.

Fig. 7A illustrates the variations of open-circuit voltage with pHs of the low concentration solution. At low solution pHs (pH<11), the open-circuit voltage of the RED stack corresponding to different salt solutions lies in the following order: NaCl>Na_3PO_4 >Na_2SO_4. When the pH of the low concentration solution is 13, the open-circuit voltages of the RED stacks with NaCl solution and Na_2SO_4 solution are similar, and both are lower than that with Na_3PO_4 solution. The open-circuit voltage of the RED stack with NaCl or Na_2SO_4 solutions decreases slowly first with increasing pH, and then drops sharply, as the OH^- of the low concentration solution hinders the anions passing through the AEMs. This effect becomes more obvious at large OH^- concentrations, resulting in a significant drop in the open-circuit voltage of the RED stack. While the open-circuit voltage of the stack with Na_3PO_4 solution increases with increasing pH_L and then drops. The ion transmembrane transport is slightly improved with increasing pH_L due to the different degrees of hydrolysis of the salt solutions on both sides of IEMs, thus enhancing the open-circuit voltage, which achieves a maximum value of 0.629 V at pH_L= 11. However, the negative impact of excessive OH^- leads to a sharp drop in the open-circuit voltage at pH_L= 13. Meanwhile, the

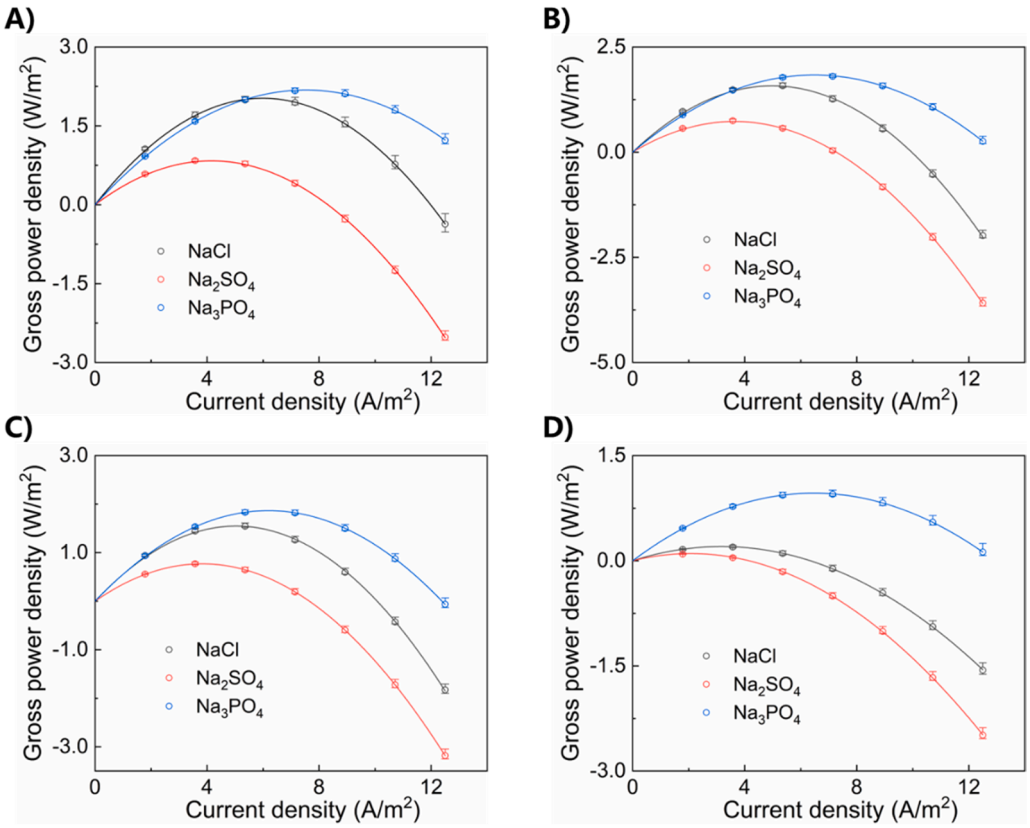

Fig. 6. Gross power density with the current density while pH_H= 7. A) pH_L= 7, B) pH_L= 9, C) pH_L= 11, and D) pH_L= 13.

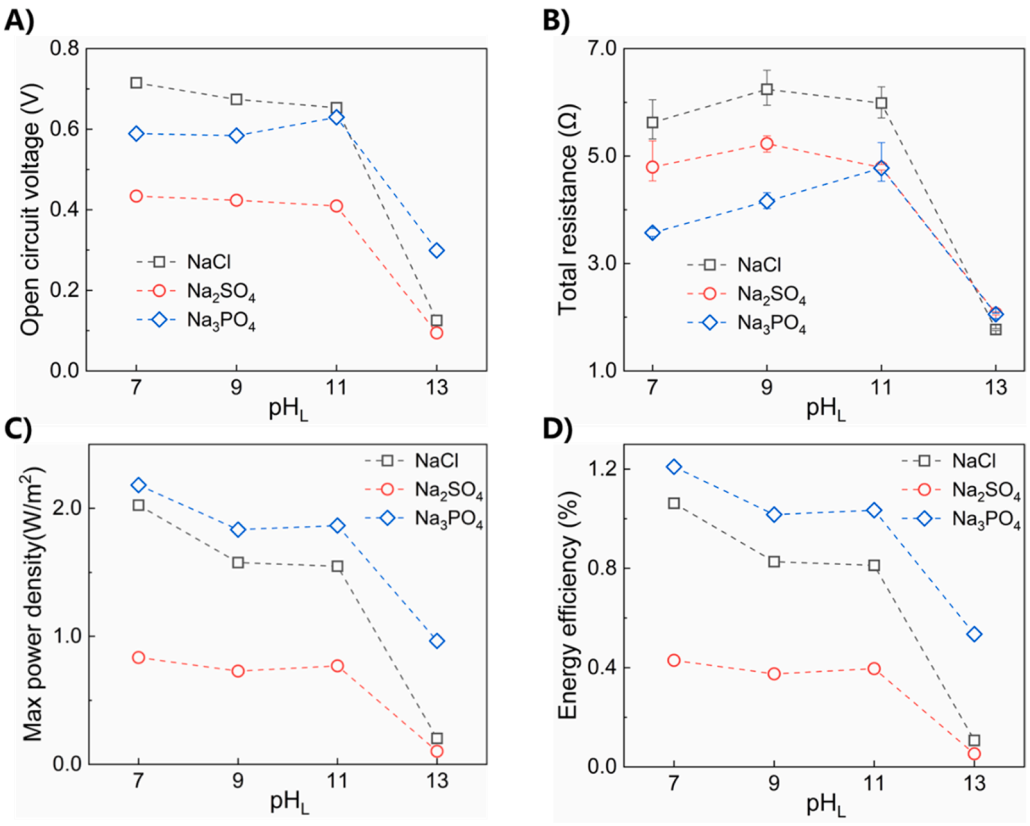

Fig. 7. Performance of the RED stack in asymmetric pH configuration while pH_H= 7.

additional cations in the low concentration side at larger pH decrease the effective transmembrane ion concentration gradient, weakening the diffusion drive of ions, which also contributes to the reduction of the open-circuit voltage of the RED stack.

Fig. 7B shows the variations of resistance with pHs of the low concentration solution. The total resistance of the RED stack is strongly influenced by the pH of the low concentration solution and salt types. When the pH of the low concentration solution is lower than 13, the RED stack with NaCl solution has the largest resistance. However, it is slightly smaller than that of the stack with Na_2SO_4 or Na_3PO_4 solutions at the low concentration solution pH= 13. When low concentration solution pH is lower than 11, the total resistance of the RED stack with Na_3PO_4 solutions is smaller than that with Na_2SO_4 solution. However, the difference is not obvious at large low concentration solution pHs. As the conductivity of the salt solution is influenced by the species and counts of ions contained, the higher the valence of the anion, the more the total amount of Na^+ in the solution, which means that the corresponding conductivity is stronger and the ohmic resistance contributed to the RED stack is smaller. The total resistance of the RED stack with different salt solutions increases with increasing low concentration solution pH and then decreases. For the RED stack with NaCl solution and Na_2SO_4 solution, the peak values of resistance (6.24 Ω and 5.23 Ω, respectively) occur at the low concentration solution pH= 9; while for the RED stack with Na_3PO_4 solution, the maximum total resistance is 4.78 Ω at the low concentration solution pH= 11.

Fig. 7C illustrates the variations of the maximum power density of the RED stack with low concentration solution pH under different salt solutions. The maximum power density of the RED stack corresponding to different salt solutions lies in the order: Na_3PO_4 >NaCl>$NaSO_4$. As the maximum power density of the stack is determined by the open-circuit voltage and total resistance, the RED stack with Na_3PO_4 solution has a higher open-circuit voltage as well as the lowest total resistance under different low concentration solution pHs, thus presenting the greatest max power density. For different salt solutions, the maximum power density of the RED stack decreases with the increasing pH of the low concentration solution. In the experiment, the inlet flow rates and the concentrations of salt solutions are kept the same for different salt solutions. The input Gibbs free energy varies rather slightly at different low concentration solution pHs, resulting in the energy conversion efficiency of the RED stack with different salt solutions presenting the same trend with the maximum power density, as shown in Fig. 7D. Overall, the higher low concentration solution pH is unfavorable to the energy conversion performance of the RED stack.

3.2.2. *Effects of pH of the high concentration solution*

The pH of the low concentration solution is kept at 7, and the pH of the high concentration solution is adjusted from 7 to 13. Fig. 8 shows the variations of the RED stack's output power density with current density under different pH values of the high concentration solution. When the pH of the high concentration solution is lower than 13, the RED stack with Na_3PO_4 solution presents the greatest output power and the largest short-circuit current. The gross power densities of the RED stack with NaCl solution and Na_2SO_4 solution are similar at small high concentration solution pHs. When the pH of the high concentration solution is adjusted to 13, the power densities of the stack with Na_2SO_4 solution and Na_3PO_4 solution are close, and the output performance of the stack with NaCl solution is rather higher than that with the other salt solutions.

Fig. 9A illustrates the variations of open-circuit voltage with pHs of the high concentration solution. The RED stack with NaCl solution has the largest open-circuit voltage under different high concentration solution pHs. When the pH of the high concentration solution is less than 11, the open-circuit voltage of the stack with Na_2SO_4 solution is the lowest, which exceeds that with Na_3PO_4 solution when the pH of the high concentration solution is larger than 11. For the RED stack with NaCl solution, the open-circuit voltage drops first with increasing pH of the high concentration solution, and then increases. When the pH of the

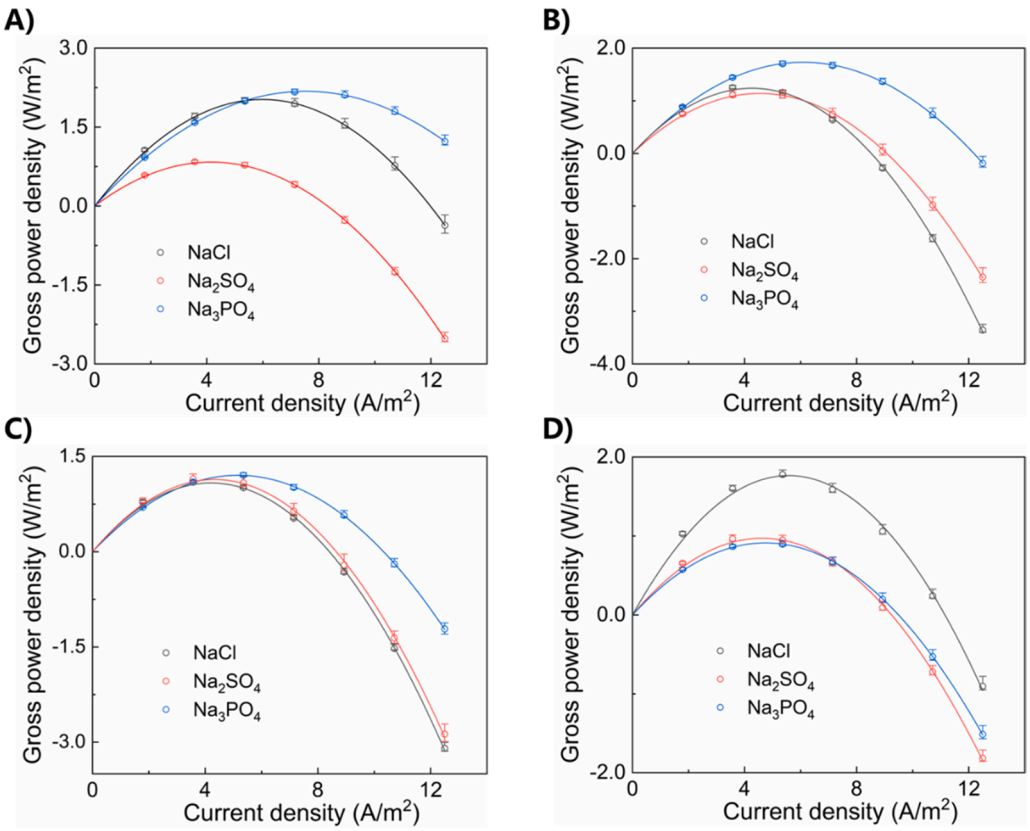

Fig. 8. Gross power density with the current density while pH_L= 7. A) pH_H= 7, B) pH_H= 9, C) pH_H= 11, and D) pH_H= 13.

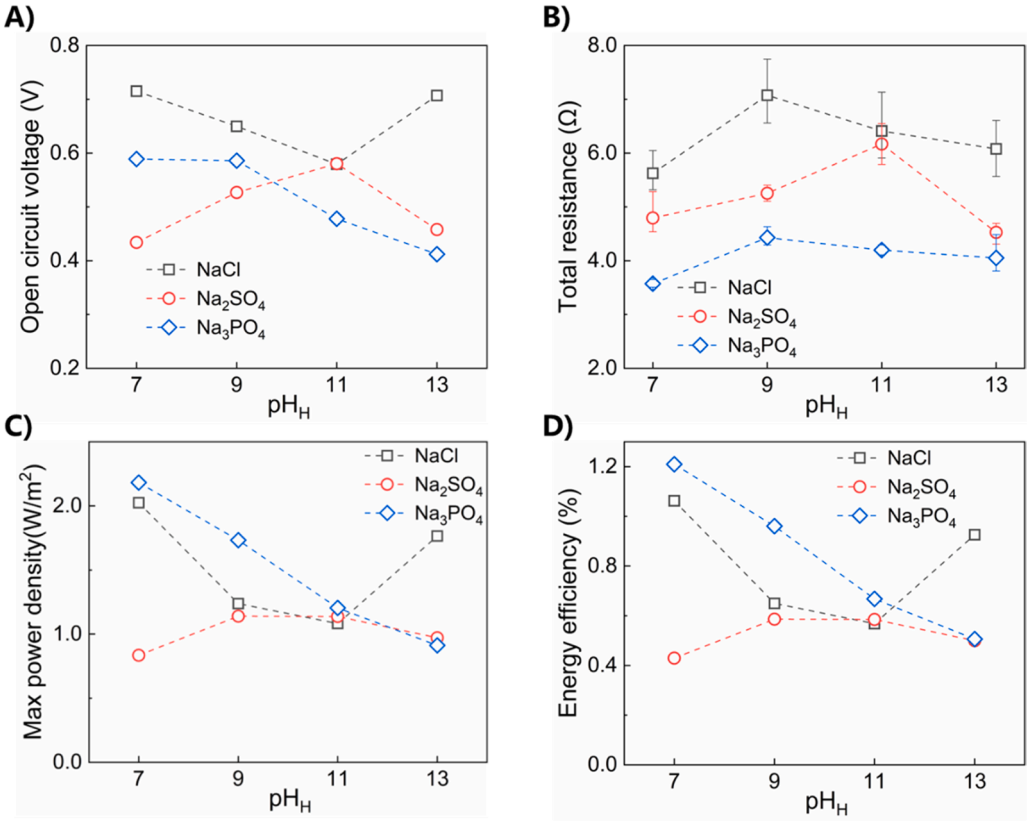

Fig. 9. Performance of the RED stack in asymmetric pH configuration while pH_L= 7.

high concentration solution is low, the amount of NaOH added is small, thus leading to a slight effect on the original transmembrane concentration ratio of Na^+. Meantime, The OH^- weakens the permeability of Cl^- through AEMs, resulting in a gradual decrease of the open-circuit voltage. The additional cations by adjusting the pH strongly increase the ratio of transmembrane ion concentration at larger pH of the high concentration solution, thus leading to the rise in the open-circuit voltage, which is 0.707 V and only slightly lower than the value of 0.715 V at pH_H= 7. For salt solutions with higher anion valences such as Na_2SO_4 and Na_3PO_4, large amounts of original Na^+ exist. The transmembrane ion concentration gradient is not so susceptible to the influence of extra cations induced by adjusting the pH of the high concentration solution. The effect of OH^- introduced is more dominant in transmembrane ion transportation. When the pH of the high concentration solution is low, the weakly alkaline environment slightly improves the permselectivity of IEMs to Na^+ and SO_4^{2-} as in the case of the symmetrical configuration, increasing the open-circuit voltage; when the pH of the high concentration solution is high, the large amount of OH^- reduces the transportation of anions across AEMs, which inhibits rise the in the open-circuit voltage of the RED stack. Therefore, the open-circuit voltage of the stack with Na_2SO_4 increases with the increasing pH of the high concentration solution and then drops, achieving a peak value of 0.580 V at pH_H= 11. For the stack with Na_3PO_4 solution, the addition of OH^- inhibits the hydrolysis of Na_3PO_4, reducing the ion activity and weakening the permeation of anions through AEMs, which accounts for the reduction of the open-circuit voltage.

Fig. 9B shows the variations of resistance with pHs of the high concentration solution. At each pH of the high concentration solution, the total resistance of the RED stack corresponding to different salt solutions is in the order: NaCl>Na_2SO_4 >Na_3PO_4. For various salt solutions, the resistance tends to increase first with the increasing pH of the high concentration solution, reach the corresponding maximum value, and then decrease. The RED stack with NaCl solution and Na_3PO_4 solution present the maximum resistances of 7.07 Ω and 4.43 Ω respectively when the pH of the high concentration solution is 9; while for the stack with Na_2SO_4 solution, the peak value of total resistance (6.17 Ω) occurs when the pH of the high concentration solution is 11.

Fig. 9C and D illustrate the maximum power density and energy efficiency of the RED stack with high concentration solution pHs under different salt solutions. For the RED stack with NaCl solution, the maximum power density decreases first with increasing high concentration solution pH, and then increases; for the RED stack with Na_2SO_4 solution, the maximum power density increases with increasing high concentration solution pH, and then decreases; for the RED stack with Na_3PO_4 solution, the maximum power density drops monotonously with increasing high concentration solution pH. The diverse performance variations for different salt solutions are mainly due to the coupling effects of open-circuit voltage and total resistance under different pH of high concentration solutions. The maximum power density of the RED stack with Na_3PO_4 solution is the greatest when the pH of the high concentration solution is less than 13, while that with NaCl solution surpasses it when the pH of the high concentration solution is 13. In the experiment, the inlet flow rates and the concentrations of salt solutions are kept the same for different salt solutions. The input Gibbs free energy varies rather slightly at various high concentration solution pHs, resulting in the energy conversion efficiency of the RED stack with different salt solutions presenting the same trend with the maximum power density, as shown in Fig. 9D. For the RED stack with Na_2SO_4 solution, an appropriate increase of pH of the high concentration solution is beneficial to improve the output power and energy conversion efficiency. While for the stack with Na_3PO_4 solution, the energy conversion performance can be significantly weakened.

4. Conclusions

In this study, the performance of the RED stack involving sodium salt solutions with anions at different valences is experimentally investigated in symmetric pH configuration (same pH for high and low concentration solutions) and asymmetric pH configuration (different pH for high and low concentration solutions). In the symmetrical pH configuration, for the 1:1 salt, increasing the pH of the solution significantly weakens the transmembrane concentration difference, thus reducing the output voltage and power density; for the 1:2 salt, the power density and energy conversion efficiency increase and then decrease due to the coupling effects of OH^- on the ion transportation through AEMs and CEMs; for the 1:3 salt, OH^- inhibits the transportation of anions by AEMs and remarkably reduces the energy conversion property. In the asymmetric pH configuration, increasing the pH of the low concentration solution reduces the transmembrane ion concentration gradient and decreases the power density and energy conversion efficiency. With increasing the pH of the high concentration solution, for the 1:1 salt, the output power and energy conversion efficiency decrease and then increase because of the coupling effects of the ion transmembrane concentration difference and OH^- on the ion migration of IEMs; for the 1:2 salt, the output power and energy conversion efficiency increase and then decrease; for the 1:3 salt, OH^- inhibits the hydrolysis of Na_3PO_4 and anion migration, leading to the decrease of power density and energy efficiency. This study may provide an experimental reference for the design and optimization of the RED stack with salinity gradient energy conversion in different pH environments.

Declaration of Competing Interest

The authors declare that they have no known competing financial interests or personal relationships that could have appeared to influence the work reported in this paper.

Acknowledgments

This work was financially supported by the National Natural Science Foundation of China (52176070).

Declaration of interest

The authors declare no competing financial interest.

References

Avci, A.H., Sarkar, P., Tufa, R.A., Messana, D., Argurio, P., Fontananova, E., et al., 2016. Effect of Mg2+ ions on energy generation by reverse electrodialysis. J. Membr. Sci. 520, 499–506.

Benneker, A.M., Rijnaarts, T., Lammertink, R.G.H., Wood, J.A., 2018. Effect of temperature gradients in (reverse) electrodialysis in the Ohmic regime. J. Membr. Sci. 548, 421–428.

Chen, X., Luo, Z., Long, R., Liu, Z., Liu, W., 2022. Impacts of transmembrane pH gradient on nanofluidic salinity gradient energy conversion. Renew. Energy 187, 440–449.

Choi, J., Kim, W.-S., Kim, H.K., Yang, S., Jeong, N.J., 2021. Ultra-thin pore-filling membranes with mirror-image wave patterns for improved power density and reduced pressure drops in stacks of reverse electrodialysis. J. Membr. Sci. 620, 118885.

Cipollina, A., Micale, G., Tamburini, A., Tedesco, M., Gurreri, L., Veerman, J., et al., 2016. 5 - Reverse electrodialysis: Applications. In: Cipollina, A., Micale, G. (Eds.), Sustainable Energy from Salinity Gradients. Woodhead Publishing, pp. 135–180.

Cui, W.-Z., Ji, Z.-Y., Tumba, K., Zhang, Z.-D., Wang, J., Zhang, Z.-X., et al., 2022. Response of salinity gradient power generation to inflow mode and temperature difference by reverse electrodialysis. J. Environ. Manag. 303, 114124.

Culcasi, A., Gurreri, L., Micale, G., Tamburini, A., 2021. Bipolar membrane reverse electrodialysis for the sustainable recovery of energy from pH gradients of industrial wastewater: performance prediction by a validated process model. J. Environ. Manag. 287, 112319.

Daniilidis, A., Vermaas, D.A., Herber, R., Nijmeijer, K., 2014. Experimentally obtainable energy from mixing river water, seawater or brines with reverse electrodialysis. Renew. Energy 64, 123–131.

Długołęcki, P., Dąbrowska, J., Nijmeijer, K., Wessling, M., 2010. Ion conductive spacers for increased power generation in reverse electrodialysis. J. Membr. Sci. 347 (1), 101–107.

Guo, H., Hu, W., Xu, Z., Guo, S., Qiao, D., Wang, X., et al., 2022. How to improve lead dioxide anodes performance in organic wastewater treatment: review and prospect. Process Saf. Environ. Prot. 164, 189–207.

Guo, Z.-Y., Ji, Z.-Y., Zhang, Y.-G., Yang, F.-J., Liu, J., Zhao, Y.-Y., et al., 2018. Effect of ions (K+, Mg2+, Ca2+ and SO42−) and temperature on energy generation performance of reverse electrodialysis stack. Electrochim. Acta 290, 282–290.
Hong, J.G., Zhang, B., Glabman, S., Uzal, N., Dou, X., Zhang, H., et al., 2015. Potential ion exchange membranes and system performance in reverse electrodialysis for power generation: a review. J. Membr. Sci. 486, 71–88.
Hong, J.G., Park, T.-W., Dhadake, Y., 2019. Property evaluation of custom-made ion exchange membranes for electrochemical performance in reverse electrodialysis application. J. Electroanal. Chem. 850, 113437.
Hsu, J.-P., Lin, S.-C., Lin, C.-Y., Tseng, S., 2017. Power generation by a pH-regulated conical nanopore through reverse electrodialysis. J. Power Sources 366, 169–177.
Hsu, J.-P., Su, T.-C., Lin, C.-Y., Tseng, S., 2019. Power generation from a pH-regulated nanochannel through reverse electrodialysis: effects of nanochannel shape and non-uniform H+ distribution. Electrochim. Acta 294, 84–92.
Hulme, A.M., Davey, C.J., Tyrrel, S., Pidou, M., McAdam, E.J., 2021. Transitioning from electrodialysis to reverse electrodialysis stack design for energy generation from high concentration salinity gradients. Energy Convers. Manag 244 (None-None).
Jang, J., Kang, Y., Han, J.-H., Jang, K., Kim, C.-M., Kim, I.S., 2020. Developments and future prospects of reverse electrodialysis for salinity gradient power generation: Influence of ion exchange membranes and electrodes. Desalination 491, 114540.
Kim, H., Yang, S., Choi, J., Kim, J.-O., Jeong, N., 2021. Optimization of the number of cell pairs to design efficient reverse electrodialysis stack. Desalination 497, 114676.
Kingsbury, R.S., Liu, F., Zhu, S., Boggs, C., Armstrong, M.D., Call, D.F., et al., 2017. Impact of natural organic matter and inorganic solutes on energy recovery from five real salinity gradients using reverse electrodialysis. J. Membr. Sci. 541, 621–632.
Kuang, Z., Zhang, D., Shen, Y., Long, R., Liu, Z., Liu, W., 2019. Bioinspired fractal nanochannels for high-performance salinity gradient energy conversion. J. Power Sources 418, 33–41.
Lacey, R.E., 1980. Energy by reverse electrodialysis. Ocean Eng. 7 (1), 1–47.
Li, J., Zhang, C., Wang, Z., Bai, Z., Kong, X., 2022. Salinity gradient energy harvested from thermal desalination for power production by reverse electrodialysis. Energy Convers. Manag. 252, 115043.
Logan, B.E., Elimelech, M., 2012. Membrane-based processes for sustainable power generation using water. Nature 488 (7411), 313–319.
Long, R., Li, B., Liu, Z., Liu, W., 2018a. Performance analysis of reverse electrodialysis stacks: channel geometry and flow rate optimization. Energy 158, 427–436.
Long, R., Li, B., Liu, Z., Liu, W., 2018a. Reverse electrodialysis: Modelling and performance analysis based on multi-objective optimization. Energy 151, 1–10.
Long, R., Kuang, Z., Liu, Z., Liu, W., 2018b. Temperature regulated reverse electrodialysis in charged nanopores. J. Membr. Sci. 561, 1–9.
Long, R., Kuang, Z., Liu, Z., Liu, W., 2019. Ionic thermal up-diffusion in nanofluidic salinity-gradient energy harvesting. Natl. Sci. Rev. 6 (6), 1266–1273.
Long, R., Luo, Z., Kuang, Z., Liu, Z., Liu, W., 2020. Effects of heat transfer and the membrane thermal conductivity on the thermally nanofluidic salinity gradient energy conversion. Nano Energy 67, 104284.
Long, R., Li, M., Chen, X., Liu, Z., Liu, W., 2021. Synergy analysis for ion selectivity in nanofluidic salinity gradient energy harvesting. Int. J. Heat. Mass Transf. 171, 121126.
Mai, V.P., Yang, R.J., 2020. Active control of salinity-based power generation in nanopores using thermal and pH effects. RSC Adv. 10 (32), 18624–18631.
Mukherjee, M., Roy, S., Bhowmick, K., Majumdar, S., Prihatiningtyas, I., Van der Bruggen, B., et al., 2022. Development of high performance pervaporation desalination membranes: a brief review. Process Saf. Environ. Prot. 159, 1092–1104.
Ortiz-Imedio, R., Gomez-Coma, L., Fallanza, M., Ortiz, A., Ibañez, R., Ortiz, I., 2019. Comparative performance of Salinity Gradient Power-Reverse Electrodialysis under different operating conditions. Desalination 457, 8–21.
Panagopoulos, A., 2021. Techno-economic assessment of minimal liquid discharge (MLD) treatment systems for saline wastewater (brine) management and treatment. Process Saf. Environ. Prot. 146, 656–669.
Pattle, R.E., 1954. Production of electric power by mixing fresh and salt water in the hydroelectric pile. Nature 174 (4431), 660 (-).
Pawlowski, S., Rijnaarts, T., Saakes, M., Nijmeijer, K., Crespo, J.G., Velizarov, S., 2017. Improved fluid mixing and power density in reverse electrodialysis stacks with chevron-profiled membranes. J. Membr. Sci. 531, 111–121.
Pitzer, K.S., Mayorga, G., 1993. Thermodynamics of Electrolytes.: II. Activity and Osmotic Coefficients for Strong Electrolytes with One or Both Ions Univalent. Molecular Structure and Statistical Thermodynamics. World Scientific, pp. 396–404.
Soliman, M.N., Guen, F.Z., Ahmed, S.A., Saleem, H., Khalil, M.J., Zaidi, S.J., 2021. Energy consumption and environmental impact assessment of desalination plants and brine disposal strategies. Process Saf. Environ. Prot. 147, 589–608.
Tedesco, M., Cipollina, A., Tamburini, A., Bogle, I.D.L., Micale, G., 2015. A simulation tool for analysis and design of reverse electrodialysis using concentrated brines. Chem. Eng. Res. Des. 93, 441–456.
Tedesco, M., Scalici, C., Vaccari, D., Cipollina, A., Tamburini, A., Micale, G., 2016. Performance of the first reverse electrodialysis pilot plant for power production from saline waters and concentrated brines. J. Membr. Sci. 500, 33–45.
Tedesco, M., Cipollina, A., Tamburini, A., Micale, G., 2017. Towards 1kW power production in a reverse electrodialysis pilot plant with saline waters and concentrated brines. J. Membr. Sci. 522, 226–236.
Tufa, R.A., Pawlowski, S., Veerman, J., Bouzek, K., Fontananova, E., di Profio, G., et al., 2018. Progress and prospects in reverse electrodialysis for salinity gradient energy conversion and storage. Appl. Energy 225, 290–331.
Veerman, J., Saakes, M., Metz, S.J., Harmsen, G.J., 2010a. Reverse electrodialysis: evaluation of suitable electrode systems. J. Appl. Electrochem. 40 (8), 1461–1474.
Veerman, J., Saakes, M., Metz, S.J., Harmsen, G.J., 2010b. Electrical power from sea and river water by reverse electrodialysis: a first step from the laboratory to a real power plant. Environ. Sci. Technol. 44 (23), 9207–9212.
Venzke, C.D., Giacobbo, A., Ferreira, J.Z., Bernardes, A.M., Rodrigues, M.A.S., 2018. Increasing water recovery rate of membrane hybrid process on the petrochemical wastewater treatment. Process Saf. Environ. Prot. 117, 152–158.
Yip, N.Y., Brogioli, D., Hamelers, H.V.M., Nijmeijer, K., 2016. Salinity gradients for sustainable energy: primer, progress, and prospects. Environ. Sci. Technol. 50 (22), 12072–12094.
Zhang, W., Han, B., Tufa, R.A., Tang, C., Liu, X., Zhang, G., et al., 2021. Tracing the impact of stack configuration on interface resistances in reverse electrodialysis by in situ electrochemical impedance spectroscopy. Front. Environ. Sci. Eng. 16 (4), 46.
Zhu, X., He, W., Logan, B.E., 2015. Reducing pumping energy by using different flow rates of high and low concentration solutions in reverse electrodialysis cells. J. Membr. Sci. 486, 215–221.